Title

Creation of entanglement and implementation of quantum logic gate operations using a three-dimensional photonic crystal single-mode cavity

Journal

Journal of the Optical Society of America B-Optical Physics, 24(2)

ISSN

0740-3224

Authors

Guney, Durdu O

Meyer, D A

Publication Date

2007-02-01

Peer reviewed

Creation of entanglement and implementation of quantum logic gate operations using a three-dimensional photonic crystal single-mode cavity

Durdu Ö. Güney

Department of Electrical and Computer Engineering, University of California, San Diego, 9500 Gilman Dr., La Jolla, California, 92093-0409

Department of Mathematics, University of California, San Diego, 9500 Gilman Dr., La Jolla, California, 92093-0112

dguney@ucsd.edu

David A. Meyer

Department of Mathematics, University of California, San Diego, 9500 Gilman Dr., La Jolla, California, 92093-0112

dmeyer@math.ucsd.edu

We solve the Jaynes-Cummings Hamiltonian with time-dependent coupling parameters under the dipole and rotating-wave approximations for a three-dimensional (3D) photonic crystal (PC) single mode cavity with a sufficiently high quality (Q) factor. We then exploit the results to show how to create a maximally entangled state of two atoms, and how to implement several quantum logic gates: a dual-rail Hadamard gate, a dual-rail NOT gate, and a SWAP gate. The atoms in all of these operations are syncronized, which is not the case in previous studies {[J. Mod. Opt. 48, 1495 (2001)], [Eur. Phys. J. D 10, 285 (2000)], [Eur. Phys. J. D 18, 247 (2002).]} in PCs. Our method has the potential for extension to N-atom entanglement, universal quantum logic operations, and the implementation of other useful, cavity QED based quantum information processing tasks.

OCIS codes: 020.5580, 200.4660, 220.4830, 230.5750, 270.5580.

1. Introduction

The superiority of quantum computing over classical computation for problems with solutions based on the quantum Fourier transform, as well as search and (quantum) simulation problems has attracted increasing attention over the last decade. Despite promising developments in theory, however, progress in physical realization of quantum circuits, algorithms, and communication systems to date has been extremely challenging. Major model physical systems include photons and nonlinear optical media, cavity QED devices, ion traps, and nuclear magnetic resonance (NMR) with molecules, quantum dots, superconducting gates, and spins in semiconductors.[1]

Quantum logic gates and quantum entanglement constitute two building blocks, among others, of more sophisticated quantum circuits and communication protocols. The latter also allows us to test basic postulates of quantum mechanics.

In this work we propose an alternative method for creating entanglement and implementing certain quantum logic gates based on single mode PC microcavities. Our scheme requires high-Q PC microcavities with Q-factor of around 10^8, and where atoms can freely propagate through the connected void regions. We consider 3D PCs for our purposes, since they are more attractive, compared to 2D PC slabs, for the realization of such high-Q microcavities. Although the fabrication of these high-Q 3D PC microcavities is currently challenging, especially in the optical frequencies, mainly due to the reduced size of the crystals at those wavelengths; in the microwave or millimeter-wave regime, where our proposed PC cavity operates ($\sim$ 50GHz), the fabrication process is relatively easier thanks to the rather macroscopic nature of the crystals at that scale. Thus, simple machining or rapid prototyping methods can be exploited to build them.[2] It is for this reason that the initial experiments on PCs were performed in the microwave region. Subsequently, much of the research concentrated on the infrared or the optical regime of the spectrum because of numerous applications which demand telecommunications wavelengths and/or miniaturization. In the less studied but also less technically challenging microwave region the Q-factor is limited by the intrinsic loss of the material.[3,4] Using an appropriate low-loss dielectric such as sapphire, for example, it has been predicted by Yablonovitch[3] that a Q-factor of more than 10^9 should indeed experimentally be achievable. M. Qi, *et al.*[5] have furthermore predicted that using interference, imprint or X-ray lithography combined with scanning-electron-beam-lithography, their layer-by-layer approach could allow the manufacturing of large area (several square centimeters) PCs which are low-cost, optical or even visible spectrum versions of 3D PC cavities similar to ours.

2. Theory

In this paper we first explore the possibility of mutually entangling two Rb atoms by exploiting their interaction, mediated by a single defect mode confined to a three-dimensional PC cavity. We then describe various logic gates that can be implemented using the same interaction. We achieve this in three steps: analysis of a single mode cavity (i) in a generic 3D PC, (ii) in a specific 2D PC and (iii) ultimately in a 3D version of the 2D PC of (ii). We assume that the defect frequency is resonant with the Rb atoms. Because the atoms are moving, the time-dependent Hamiltonian (Jaynes-Cummings Model) for this interaction in the dipole and rotating wave approximations is

$$H(t) = \frac{\hbar\varpi}{2}\sum_j \sigma_z^j + \hbar\varpi\alpha^\dagger\alpha + \hbar\sum_j [G_j(t)\sigma_+^j\alpha + h.c.] \tag{1}$$

where the summation is over two atoms, A and B, ω is the resonant frequency, σ_z is the z-component of the Pauli spin operator and $\sigma_\pm$ are atomic raising and lowering operators. α and $\alpha^\dagger$ are photon destruction and construction operators, respectively. The time-dependent coupling parameters can be expressed as[6]

$$G_j(t) = \Omega_0 f_j(t)\cos(\zeta_j) \tag{2}$$

where Ω_0 is the peak atomic Rabi frequency over the defect mode and $f_j(t)$ is the spatial profile of the defect state observed by the atom j at time t. ζ_j is the angle between the atomic dipole moment vector, $\mu_{\mathbf{eg}}^j$, for atom j and the mode polarization at the atom location. For the rest of the paper $\cos\zeta_A = 1$, and $p = \cos\zeta_B$ will be a parameter that we adjust to effect desired interactions between atoms A and B.

We ignore the resonant dipole-dipole interaction (RDDI), because the atoms have their transition frequencies close to the center of a wide photonic band gap (PBG) and the distance between them is always sufficiently large that RDDI effect is not significant.[7,8]

Initially we prepare one of the atoms, A, in the excited state and the cavity is left in its vacuum state, so

$$|\Psi(0)\rangle = |100\rangle, \tag{3}$$

where the tensor factors describe the states of atom A, atom B, and the cavity, successively.

The PC should be designed to allow the atoms to go through the defect. This can be achieved by injecting atoms through the void regions of a PC with a defect state of acceptor type. Since the spontaneous emission of a photon from the atoms is suppressed in the periodic region of the crystal, no significant interaction occurs outside the cavity. When the atoms enter the cavity, the interaction between the atoms is enhanced by the single mode cavity. This atom-photon-atom interaction allows us to design an entanglement process between atoms.

Given the initial state, Eq. (3), the state of the system at time t should be in the form

$$|\Psi(t)\rangle = a(t)|100\rangle + b(t)|010\rangle + \gamma(t)|001\rangle \tag{4}$$

to satisfy the probability and energy conservation. We will show analytically that the amplitudes at time t can be expressed in terms of the coupling parameters and the velocities of the atoms.

We can write the Schrödinger equation for the time-evolution operator in the form[9]

$$i\hbar\frac{\partial}{\partial t}U(t,t_0) = H(t)U(t,t_0). \tag{5}$$

In the basis $\{|100\rangle, |010\rangle, |001\rangle\}$, the matrix elements of the Hamiltonian, Eq. (1), in the rotating wave approximation, are

$$H_{11} = H_{12} = H_{21} = H_{22} = H_{33} = 0 \tag{6}$$

$$H_{13} = H_{31} = \hbar G_A(t) \tag{7}$$

$$H_{23} = H_{32} = \hbar G_B(t). \tag{8}$$

The Hamiltonian operators $H(t)$ and $H(t')$ commute for $t' \neq t$, if $G_B(t)$ is a constant multiple p of $G_A(t)$. This condition can be satisfied easily by the appropriate orientation of atomic dielectric moment of the incoming atoms with respect to the electric field in Eq. (2). Then the formal solution to Eq. (5) becomes

$$U(t,t_0) = \exp[-\frac{i}{\hbar}\int_{t_0}^{t} \mathrm{d}\tau H(\tau)] = \exp(-\frac{i}{\hbar}I), \tag{9}$$

where I is defined as the integral of the Hamiltonian operator. By expanding the exponential, Eq. (9), we obtain

$$U(t,t_0) = 1 + (\frac{-i}{\hbar})I + \frac{1}{2!}(\frac{-i}{\hbar})^2 I^2 + \cdots + (\frac{1}{n!})(\frac{-i}{\hbar})^n I^n + \cdots \tag{10}$$

Multiplying Eq. (10) by the initial state $|100\rangle$ from the right and comparing with Eq. (4) gives

$$a(t) = 1 + G_A^2 \sum_{n=1}(-1)^n \frac{1}{2n!}(G_A^2 + G_B^2)^{n-1} \tag{11}$$

$$b(t) = G_A G_B \sum_{n=1}(-1)^n \frac{1}{2n!}(G_A^2 + G_B^2)^{n-1} \tag{12}$$

$$\gamma(t) = iG_A \sum_{n=1}(-1)^n \frac{1}{(2n-1)!}(G_A^2 + G_B^2)^{n-1}, \tag{13}$$

where we have defined

$$G_j = \int_{t_0}^{t} G_j(\tau)d\tau. \tag{14}$$

Recognizing the Taylor series for sine and cosine allows us to rewrite equations (11)–(13) as

$$a(t) = 1 + \frac{G_A^2}{G_A^2 + G_B^2}[\cos(G_A^2 + G_B^2)^{1/2} - 1] \tag{15}$$

$$b(t) = \frac{G_A G_B}{G_A^2 + G_B^2}[\cos(G_A^2 + G_B^2)^{1/2} - 1] \tag{16}$$

$$\gamma(t) = -i\frac{G_A}{(G_A^2 + G_B^2)^{1/2}} \sin(G_A^2 + G_B^2)^{1/2}. \tag{17}$$

For a single initially excited atom, A, passing across the cavity we can set $G_B = 0$ in equations (15)–(17), which gives the same result as Eq. (15) of Ref. [10]. The exact solution for the time-independent problem of N identical two level atoms with a resonant single mode quantized field given in Ref. [11] could be helpful to generalize our results to N-atom case, see for example Ref. [7].

Absent a rigorous calculation of the defect mode in the three-dimensional PC, which we postpone until §4, let us first assume a generic spatial profile for the mode, which oscillates and decays exponentially. Thus, $f_j(t)$ in Eq. (2) can be expressed as[6]

$$f_j(t) = \exp(-|V_j t - L|/R_{\rm def}) \cos[\frac{\pi}{l}(V_j t - L)], \tag{18}$$

where V_j, L, $R_{\rm def}$, and l are the velocity of atom j, the total path length of the atoms, the defect radius, and the lattice constant of the PC, respectively.

We choose the velocities of the atoms to be the same, $V_j = V$, with 150m/s $< V <$ 650m/s, a typical velocity range appropriate for both experiments and our calculations. Setting the atoms to have the same velocity has two immediate advantages: First, it makes the Hamiltonians at different times commute, since the coupling parameters of the atoms differ by only a constant factor [see Eq. (2)], and thus greatly simplifies the analysis. Second, it synchronizes the atoms, providing cyclical readout that could also be synchronized with the cycle time of a quantum computer.[12] These features are not present in previous studies.[6,7,13]

It was shown by E. Hagley, *et al.*[14] in 1997 that atomic velocity resolution could be as small as 0.4m/s in experiments, which means that our proposed entangler and logic gates are rather robust and insensitive to experimental velocity fluctuations. In fact, with our design the velocity resolution of the atomic pairs can be further relaxed up to slightly more than ±1m/s, increasing the efficiency of the system at the expense of less than 1% deviation in the output probability amplitudes.

Using equations (15)–(18) we can express the asymptotic probability amplitudes, $a(t)$ and $b(t)$, as functions of V and p. Fig. 1a illustrates $a(V,p)$, when the initial state is $|100\rangle$. The result for $b(V,p)$ (or $a(V,p)$), if the initial state is $|100\rangle$ (or $|010\rangle$), is displayed in Fig. 1b. Note that Fig. 1b illustrates two probability amplitudes simultaneously. This is a consequence of the symmetry in Eq. (16). To compute these surfaces we used the asymptotic (constant)

values of the G_j, which describe the accumulated atom-cavity coupling during the interaction time [(see Eq. (14)]. Once this interaction ceases to occur as the atoms leave the cavity, those asymptotic values of the G_j are reached, and thus must be used in equations (15)-(17).

Fig. 2a illustrates a slice from the surface in Fig. 1a where the velocity of the atoms is $V = 433\text{m/s}$. Note that we obtain the maximally entangled state,

$$|\Psi_{10}\rangle \cong \frac{|10\rangle + |01\rangle}{\sqrt{2}}, \tag{19}$$

up to an overall phase, -1, when the velocity of the atoms, $V = 433\text{m/s}$, and the initial state is $|100\rangle$. Similarly if we keep the velocities of the atoms the same but set the atom B to be excited initially (i.e., the initial state is $|010\rangle$), we obtain the slice in Fig. 2b and thus the maximally entangled state,

$$|\Psi_{01}\rangle \cong \frac{|10\rangle - |01\rangle}{\sqrt{2}}, \tag{20}$$

up to the same overall phase factor as in Eq. (19). [In equations (19) and (20), and in the following, we omit the cavity state in the kets, since it factors out and does not contribute to the logic operations with which we are concerned.]

Fig. 3 shows the coupling parameters calculated in the reference frame of the atoms as a function of time, $G_j(t)$, with the chosen values of Ω_0, L, R_{def}, and l. The solid red curve and blue dashed curve correspond to atoms A and B, respectively. The total interaction time is less than 20ns.

The probabilities $|a(t)|^2$, $|b(t)|^2$ and $|\gamma(t)|^2$ from equations (15)–(17) are graphed in Fig. 4. Fig. 4a shows the evolution of the probabilities when the initial state is $|100\rangle$. Note that the cavity is disentangled from the atoms and we end up with the final state, Eq. (19). On the other hand, if the initial state is $|010\rangle$, the time evolution of the probabilities is illustrated in Fig. 4b. Note that the final state in this setting becomes Eq. (20), since the cavity is again disentangled. From equations (19) and (20) it is clear that the quantum system we have described not only entangles the atoms but *also operates as a dual-rail Hadamard gate*[1]*, up to an overall phase.*

Using the same quantum system one can also design a dual-rail NOT gate under certain conditions. If we set $V_A = V_B = 565\text{m/s}$, for example, we obtain the following logical transformations, up to an unimportant global phase factor, which define a dual-rail NOT gate (see Fig. 5):

$$|10\rangle \mapsto |01\rangle \tag{21}$$

$$|01\rangle \mapsto |10\rangle. \tag{22}$$

Furthermore, using the Hamiltonian, Eq. (1), it can be shown that a $|00\rangle$ initial state only gains a deterministic phase factor of -1 in the interaction picture. Once the conditions,

equations (21) and (22), are satisfied, a $|11\rangle$ initial state is transformed into itself up to the same global phase as the states in equations (21) and (22). Thus, including these as possible initial states, our dual-rail NOT gate also operates as a SWAP gate up to the relative phase of the $|00\rangle$ state. Similar analysis shows that a dual-rail Z gate is also possible for certain parameter choices.

3. Two-dimensional Photonic Crystals

In the preceding analysis we have assumed the generic form, Eq. (18), for the spatial profile of the defect mode in order to demonstrate that, in principle, PC microcavities can be used as entanglers, and more specifically, as certain logic gates. In the following we apply these ideas to two- and finally real three-dimensional photonic crystal microcavity designs, to show that implementations of these quantum devices are indeed possible in these photonic systems. As the authors of Ref. [7] observe, however, "a rigorous calculation of the electromagnetic field in the presence of a defect in a 3D photonic crystal can be a difficult task". In the following we address this task systematically.

First we consider a 2D photonic crystal design with a triangular lattice of dielectric rods with dielectric constant of 12 (i.e., silicon) in Fig. 6. The radius of the rods is $0.175l$, where l is the lattice constant. The symmetry is broken in the center by introducing a defect with reduced rod-radius of $0.071l$ to form the microcavity of our quantum system. We assume that the atoms A and B travel along the dashed green lines shown in Fig. 6a, although any two of the obvious paths shown by dashed lines (or any void regions with line of sight to the cavity) work as well.

We should note that the 2D cavity is only designed for preliminary purposes. Since it assumes infinite height, it cannot be intended for actual implementation of our entangler or logic operations. However, the real 3D structure to be fabricated, described in §4, is sufficiently closely related to the 2D cavity designed in this section that the mode profiles along the 1D atomic trajectories in the 2D cavity overlap to a great extent with those of the 3D cavity. Regardless of the lack of vertical confinement in this preliminary 2D design, designing it first reduces the extensive computational resources needed in more sophisticated 3D logic designs.

In order to find the probability amplitudes for the atoms as a function of time while travelling through the crystal, we need to calculate the coupling parameters in Eq. (14) and substitute them in equations (15)–(17). Once we obtain the probability amplitudes, we can demonstrate entanglement creation and design logic gates as before. We also note that the quality factor of the cavity should be high enough that the interaction time (i.e., the logic operation time) is much less than the photon lifetime in the cavity. Below we show that typical logic operations take 50μs for the Hadamard gate and 30μs for the NOT or the

SWAP gate. Thus a quality factor of 10^8 should be sufficient for reliable gate operations in real 3D PC microcavities. Since our preliminary 2D PC cavity is not realistic, however, only an in-plane Q-factor of the same value is taken into consideration to match the mode profiles along the atomic trajectories in both 2D and 3D. To achieve this matching the Q-factor of the cavity could be increased exponentially with additional periods of rods[15] in Fig. 6a. We observe, however, that the spatial profile of the mode in Fig. 6b does not change significantly (and hence degrade the gate) after a certain number of periods. Thus, the exact number of periods required for a quality factor of 10^8 is not essential to demonstrate our main goal in this paper, namely that such logic operations and entanglement creation are indeed possible in these photonic crystal structures.

In our generic profile, Eq. (18), the coupling parameter is assumed to be real. For generality, however, we must allow it to be a complex parameter. Thus, the interaction part of the Hamiltonian, Eq. (1), for a single-atom cavity interaction can be written as[16–19]

$$H_I = \hbar|g(\mathbf{r})|(\alpha^\dagger\sigma_- + \alpha\sigma_+), \tag{23}$$

by incorporating a complex coupling parameter $g(\mathbf{r})$ into Eq. (1).

In a photonic crystal we can express the atom-field coupling parameter[16,20] at the position of atom j, as

$$g(\mathbf{r}_j) = g_0\Psi(\mathbf{r}_j)\cos(\zeta_j) \tag{24}$$

where g_0 and $\Psi(\mathbf{r}_j)$ are defined as:

$$g_0 \equiv \frac{\mu_{eg}}{\hbar}\left(\frac{\hbar\omega}{2\varepsilon_0\varepsilon_m V_{\text{mode}}}\right)^{1/2} \tag{25}$$

$$\Psi(\mathbf{r}_j) \equiv E(\mathbf{r}_j)/|E(\mathbf{r}_m)|. \tag{26}$$

$\mathbf{r}_m$ denotes the position in the dielectric where $\varepsilon(\mathbf{r})|E(\mathbf{r})|^2$ is maximum and ε_m is defined as the dielectric constant at that point. The cavity mode volume, V_{mode}, is given by

$$V_{\text{mode}} = \frac{\iiint \varepsilon(\mathbf{r})|E(\mathbf{r})|^2 \mathrm{d}\mathbf{r}}{\varepsilon_m|E(\mathbf{r}_m)|^2}. \tag{27}$$

Using the block iterative plane-wave expansion method[21] we found the normalized frequency of the cavity mode shown in Fig. 6b to be $0.3733c/l$. By setting $l = 2.202$mm, we tune the resonant wavelength to 5.9mm. At this wavelength, μ_{eg} for the Rb atom is 2×10^{-26}Cm.[6] Since we observe that the energy density is concentrated in the center of the cavity, ε_m in equations (25) and (27) becomes 12. On the other hand, $\cos(\zeta_j)$ in Eq. (24) can be safely assumed constant for each atom, because our cavity mode is a transverse-magnetic (TM) mode and its electric field polarization direction can always be assumed to have a constant angle with the atomic dipole moment vector, $\mu_{\mathbf{eg}}{}^j$. We can compute the coupling

parameters as functions of time in the reference frame of the moving atoms, as shown in Fig. 7. The tails of the coupling parameter functions do not contribute significantly to the results due to exponential decay away from the cavity.

With these settings Fig. 8 demonstrates an entangler which operates as a dual-rail Hadamard gate. If the initial state is $|10\rangle$ (i.e., atom A is excited), we end up with state $|\Psi_{10}\rangle$ [see Eq. (19) above and Fig. 8a]. If atom B is initially excited (i.e., the initial state is $|01\rangle$), however, we obtain the state $|\Psi_{01}\rangle$, up to an unimportant global phase factor of -1 [see Eq. (20) above and Fig. 8b] as the output of the logic gate.

In order to get the system to act as a dual-rail NOT gate, we simply set the velocities of the atoms to be $V_A = V_B = 490$m/s. The evolution of the probability amplitudes for the atoms is shown in Fig. 9. When the excitation is initially at atom A (or at atom B), it is transferred to atom B (or atom A). Note that we also get an unimportant phase factor of -1 in the output. Furthermore, as explained above, the input states $|00\rangle$ (or $|11\rangle$) are not transformed into different states, and only $|00\rangle$ gains a different phase factor of $+1$. If this phase problem with the $|00\rangle$ state were solved, the system could also be exploited as a SWAP gate.

4. Three-dimensional Photonic Crystals

Although the implementation of logic gates in 2D photonic crystals looks promising, in reality we need 3D devices. The 2D analysis is useful, however, for reducing the substantial computation required for analyzing more realistic 3D structures, because there is great similarity between the modes allowed in these 2D crystals and in their carefully chosen 3D counterparts (see Fig. 10), which we describe next.

To engineer logic operations in 3D photonic crystals, we employ the structure[5,22,23] shown in Fig. 10a. The 3D photonic crystal we have chosen has various advantages over others[24–26]: emulation of 2D properties in 3D[5,23], polarization of the modes, and simplified design and simulation. It consists of alternating layers of a triangular lattice of air holes and a triangular lattice of dielectric rods, where the centers of the holes are stacked along the [111] direction of the face-centered cubic (fcc) lattice. The parameters for the crystal are given in the caption of Fig. 10a. Using the block iterative plane-wave expansion method[21], we calculate that the structure exhibits a 3D band gap of over 20%, across the frequency range of $0.507c/l$–$0.623c/l$.

As in the 2D geometry, we introduce a defect by reducing the radius of a rod inside the crystal as shown in Fig. 10b. Using the supercell method we can compute that this cavity supports only a single mode with a frequency of $0.539c/l$. Setting $l = 3.18$mm tunes the cavity mode to the atomic transition wavelength of 5.9mm. Thus we can design a 3D single-mode cavity for our system to operate as the desired quantum logic gates.

The spatial profile for the electric field of the mode is shown in Figs. 10c and 10d. Note

that it has a similar profile to its 2D counterpart in Fig. 6b, where the energy density is also maximized in the center of the cavity. It is this similarity which simplifies our design and analysis for the 3D case.

In our designs, although the maximum field intensity is concentrated in high-dielectric regions, the resultant atom-cavity interaction is sufficient to achieve our goals. Cavities maximizing the field intensity in low-index regions, where atoms can strongly interact with the mode, could lead to higher performance. However, from the design and implementation perspective we find the former more appropriate. Some of the drawbacks of the latter can be stated as follows: If we remove the dielectric completely in the center of the defect to maximize the field intensity in air, then the defect frequency would be close to the band edge, which would thus strengthen the otherwise negligible RDDI mechanism.[7] If we use a holey lattice, on the other hand, emulating the 2D PBG inside a 3D crystal and simultaneously allowing the free passage of atoms, without interfering with the dielectric backbone of the 3D crystal, would complicate the design considerably. Nevertheless, further optimization of the proposed structure could be possible.

We can quantify[23] the TM-polarization of the mode in a plane as:

$$P \equiv \frac{\int \mathrm{d}^2\mathbf{r}|E_z(\omega;\mathbf{r})|^2}{\int \mathrm{d}^2\mathbf{r}|\mathbf{E}(\omega;\mathbf{r})|^2}. \tag{28}$$

We compute that P is almost 0.99 in the defect plane shown in Fig. 10b for the spatial profile exhibited in Figs. 10c and 10d. Thus it is safe to assume a TM polarized mode in the system Hamiltonian, because this doesn't affect the probability amplitudes significantly in the microwave regime, for the parameters we have chosen.

The coupling parameters as function of time in the reference frame of the atoms are shown in Fig. 11, where the velocities of the atoms are both set to $V = 353\mathrm{m/s}$, with $p = 0.414$.

In Fig. 12 we demonstrate the 3D version of our 2D dual-rail Hadamard gate, which also acts as an atomic entangler. Just as in the 2D case, if the initial excitation is on atom A, the resulting state is $|\Psi_{10}\rangle$ [see Eq. (19) above] as shown in Fig. 12a, while if it is on atom B the output state is $|\Psi_{01}\rangle$ [see Eq. (20) above] as displayed in Fig. 12b, up to an unimportant global phase of -1. The interaction between atom A and B is mediated by the photonic qubit when the parameters are set correctly.

We set the velocity of both atoms to $V_A = V_B = 459\mathrm{m/s}$ to obtain a dual-rail NOT gate in the 3D photonic crystal, up to an unimportant global phase factor, -1. The probability amplitude evolution of the atoms is displayed in Fig. 13.

The excitation of the excited atom is transferred to the ground state atom with the help of the photonic qubit allowed in the designed cavity. Note that because of the symmetry of the problem, the $b(t)$s in Figs. 5a, 9a and 13a are indeed approximately the same as the $a(t)$s of Figs. 5b, 9b and 13b, respectively. Furthermore, for the same reason as in the 2D case,

analyzed in the previous section, our 3D dual-rail NOT gate also operates as a SWAP gate up to some deterministic phase. That is,

$$|00\rangle \mapsto -|00\rangle \tag{29}$$

$$|01\rangle \mapsto |10\rangle \tag{30}$$

$$|10\rangle \mapsto |01\rangle \tag{31}$$

$$|11\rangle \mapsto |11\rangle. \tag{32}$$

Note also that the values of the velocities of the atoms, and g_0, for the 2D logic gates are within 10% of those in the 3D gates. This is a consequence of the fact that the localized modes allowed in 2D and 3D cavities have more than 90% overlap in their spatial profiles.[23] Thus our results are also consistent with Ref. [23] and justify first investigating the 2D case.

5. Conclusions

To summarize, photonic band gap materials could be especially promising as robust quantum circuit boards for the delicate next generation quantum computing and networking technologies. The high quality factor and extremely low mode volume achieved successfully in microcavities have already made photonic crystals an especially attractive paradigm for quantum information processing experiments in cavity QED.[6,7,27] In our paper we have extended this paradigm by solving analytically the Jaynes-Cummings Hamiltonian under the dipole and rotating wave approximations for two synchronized two-level atoms moving in a photonic crystal and by applying the solution to produce the two maximally entangled states in equations (19) and (20). We have also demonstrated the design of quantum logic gates, including dual-rail Hadamard and NOT gates, and SWAP gate operations. Our proposed system is quite tolerant to calculation and/or fabrication errors, in the sense that most errors remaining after the design can be corrected by simply experimentally adjusting the velocity or the angle between the atomic moment vector of atom B and the mode polarization. Our technique could not only be generalized to N-atom entanglement[7] but also has potential for universal quantum logic gates, atom-photon entanglement processes, as well as the implementation of various, useful cavity QED based quantum information processing tasks. We should also mention the methodological result that due to the emulation of 2D photonic crystal cavity modes in 3D photonic crystals[5,23], one can design the more sophisticated circuit first in 2D to reduce the difficulty of the 3D computations, where typically much more computational power is needed.

Acknowledgments

This work was supported in part by the National Security Agency (NSA) and Advanced Research and Development Activity (ARDA) under Army Research Office (ARO) Grant No. DAAD19-01-1-0520, by the DARPA QuIST program under contract F49620-02-C-0010, and by the National Science Foundation (NSF) under grant ECS-0202087.

References

1. M. A. Nielsen and I. L. Chuang, *Quantum Information and Quantum Computing* (Cambridge University, 2000).
2. C. M. Soukoulis, "The history and a review of the modelling and fabrication of photonic crystals," Nanotechnology **13,** 420–423 (2002).
3. E. Yablonovitch, "Photonic crystals," J. Mod. Opt. **41,** 173-194 (1994).
4. Ekmel Özbay, Nanotechnology Research Center, Bilkent University, Ankara, Turkey, 06800 (personal communication, 2006).
5. M. Qi, E. Lidorikis, P. T. Rakich, S. G. Johnson, J. D. Joannopoulos, E. P. Ippen, and H. I. Smith, "A three-dimensional optical photonic crystal with designed point defects," Nature (London) **429,** 538–542 (2004).
6. N. Vats and T. Rudolph, "Quantum information processing in localized modes of light within a photonic band-gap material," J. Mod. Opt. **48,** 1495–1502 (2001).
7. M. Konopka and V. Buzek, "Entangling atoms in photonic crystals," Eur. Phys. J. D **10,** 285–293 (2000).
8. S. John and J. Wang, "Quantum optics of localized light in a photonic band gap," Phys. Rev. B **43,** 12772–12789 (1991).
9. J. J. Sakurai, *Modern Quantum Mechanics* (Addison-Wesley, 1994).
10. J. D. Joannopoulos, R. D. Meade, and J. N. Winn, *Photonic Crystals: Molding the Flow of Light* (Princeton University, 1995).
11. M. Tavis and F. W. Cummings, "Exact solution for N-molecule-radiation field Hamiltonian," Phys. Rev. **170,** 379–384 (1968).
12. T. B. Pittman and J. D. Franson, "Cyclical quantum memory for photonic qubits," Phys. Rev. A **66,** 062302–062305 (2002).
13. D. G. Angelakis and P. L. Knight, "Testing Bell inequalities in photonic crystals," Eur. Phys. J. D **18,** 247–250 (2002).
14. E. Hagley, X. Maitre, G. Nogues, C. Wunderlich, M. Brune, J. M. Raimond, and S. Haroche, "Generation of Einstein-Podolsky-Rosen pairs of atoms," Phys. Rev. Lett. **79,** 1-5 (1997).

15. P. R. Villeneuve, S. Fan, and J. D. Joannopoulos, "Microcavities in photonic crystals: mode symmetry, tunability, and coupling efficiency," Phys. Rev. B **54,** 7837–7842 (1996).
16. Jelena Vuckovic, Ginzton Laboratory, Stanford University, Stanford, CA, 94305 (personal communication, 2004).
17. H. J. Kimble, "Strong interactions of single atoms and photons in cavity QED," Physica Scripta **T76,** 127–137 (1998).
18. S. Haroche and J. M. Raimond, "Manipulation of nonclassical field states," in *Cavity Electrodynamics,* P. Berman, eds. (Academic, San Diego, Calif., 1994), pp. 126–127.
19. Y. Yamamoto and A. Imamoglu, *Mesoscopic Quantum Optics* (Wiley-Interscience, 1999).
20. R. J. Glauber and M. Lewenstein, "Quantum optics of dielectric media," Phys. Rev. A **43,** 467–491 (1991).
21. S. G. Johnson and J. D. Joannopoulos, "Block-iterative frequency-domain methods for Maxwell's equations in a planewave basis," Opt. Express **8,** 173–190 (2001).
22. S. G. Johnson and J. D. Joannopoulos, "Three-dimensionally periodic dielectric layered structure with omnidirectional photonic band gap," Appl. Phys. Lett. **77,** 3490–3492 (2000).
23. M. L. Povinelli, S. G. Johnson, S. Fan, and J. D. Joannopoulos, "Emulation of two-dimensional photonic crystal defect modes in a photonic crystal with a three-dimensional photonic band gap," Phys. Rev. B **64,** 075313–075320 (2001).
24. S. Fan, P. R. Villeneuve, R. D. Meade, and J. D. Joannopoulos, "Design of three-dimensional photonic crystals at submicron lengthscales," Appl. Phys. Lett. **65,** 1466–1468 (1994).
25. K. H. Dridi, "Intrinsic eigenstate spectrum of planar multilayer stacks of two-dimensional photonic crystals," Opt. Express **11,** 1156–1165 (2003).
26. K. H. Dridi, "Mode dispersion and photonic storage in planar defects within Bragg stacks of photonic crystal slabs," J. Opt. Soc. Am. B **21,** 522–530 (2004).
27. J. Vuckovic, M. Loncar, H. Mabuchi, and A. Scherer, "Design of photonic crystal microcavities for cavity QED", Phys. Rev. E **65,** 016608–016618 (2001).

List of Figure Captions

Fig. 1. Probability amplitudes as a function of the velocity and p. Surfaces (a) $a(V,p)$ and (b) $b(V,p)$ (or $a(V,p)$) if the initial state is $|100\rangle$ (or $|010\rangle$). (c) Surface $b(V,p)$, if the system is initially prepared in the $|010\rangle$ state.

Fig. 2. Slices from each surface in Fig. 1. (a) Probability amplitudes $a(V,p)$—red—and $b(V,p)$—dashed blue—with $V = 433$m/s. The entangled state, Eq. (19), is obtained at $p = 0.414$. (b) Probability amplitudes $a(V,p)$—dashed blue—and $b(V,p)$—red—with the same velocity, $V = 433$m/s. The entangled state, Eq. (20), is observed at the same value, $p = 0.414$.

Fig. 3. Coupling parameters in the reference frame of moving atoms with velocities $V = 433$m/s at $p = 0.414$. $\Omega_0 = 11 \times 10^9$Hz, $\omega = 2.4 \times 10^{15}$Hz, $l = 1.6\frac{\pi c}{\omega}$, $L = 10l$, $R_{\rm def} = l$.[6] Atom A experiences the coupling parameter shown with the red solid curve and atom B the one shown with dashed blue.

Fig. 4. Time evolution of the probabilities showing the final entanglement when (a) the initial state is $|100\rangle$ and (b) $|010\rangle$.

Fig. 5. Time evolution of the probabilities that leads to a dual-rail NOT (Pauli σ_x) logic operation when (a) the initial state is $|100\rangle$ and (b) $|010\rangle$.

Fig. 6. (a) A single-mode microcavity in a 2D photonic crystal with a triangular lattice (see the text for details). (b) The corresponding electric field spatial profile for the transverse-magnetic (TM) mode allowed in the cavity.

Fig. 7. Normalized coupling parameters (i.e., divided by g_0) in the reference frame of moving atoms with velocities $V = 374$m/s at $p = 0.414$, where g_0 is found to be 2.765MHz. Blue and red curves correspond to normalized coupling strengths for atoms A and B, respectively.

Fig. 8. Probability amplitudes for entangled atoms created by a dual-rail Hadamard operation in the 2D photonic crystal (see Fig. 6) (a) when atom A is initially in the excited state and (b) when atom B is initially in the excited state. $a(t)$, $b(t)$ and $\gamma(t)$ are probability amplitudes for the states $|100\rangle$, $|010\rangle$ and $|001\rangle$, respectively.

Fig. 9. Probability amplitudes for atom A and B under the dual-rail NOT operation in the 2D photonic crystal when initially (a) atom A is excited only and (b) atom B is excited only.

Fig. 10. (a) Top view of the 3D photonic crystal with fcc lattice. It consists of alternating layers of a triangular lattice of air holes and a triangular lattice of dielectric rods (for details of the structure, see Refs. [5, 22, 23]). The nearest-neighbor spacing within either a hole or rod layer is $\frac{1}{\sqrt{2}}l$, where l is the fcc lattice constant. The hole and rod radii are $0.293l$ and $0.124l$, respectively. The thicknesses of a hole layer and a rod layer are taken to be $0.225l$ and $0.354l$, respectively. Silicon is assumed as the high-index material of dielectric constant 12. (b) Horizontal cross-section of the crystal. Dashed lines show the obvious paths atoms can travel. In our simulations we assumed the path shown by the dashed yellow line. A defect is

introduced by reducing the radius of the middle rod down to $0.050l$ to hold a single mode in the cavity. The (c) real part and (d) imaginary part of the electric-field of the TM mode allowed in the cavity at a particular instant in time with the frequency of $0.539c/l$. The imaginary part is half a period later.

Fig. 11. Coupling parameters in the reference frame of the moving atoms with both velocities $V = 353$m/s, and $p = 0.414$, where g_0 is found to be 2.899MHz. Blue and red curves correspond to normalized coupling strengths for atoms A and B, respectively.

Fig. 12. Probability amplitudes for the entangled atoms under dual-rail Hadamard operation in the 3D photonic crystal (see Fig. 10) when (a) atom A is initially in the excited state and (b) atom B is initially in the excited state. $a(t)$, $b(t)$ and $\gamma(t)$ are probability amplitudes for the states $|100\rangle$, $|010\rangle$ and $|001\rangle$, respectively.

Fig. 13. Probability amplitudes for atoms A and B under the dual-rail NOT operation in the 3D photonic crystal when initially (a) only atom A is excited and (b) only atom B is excited.

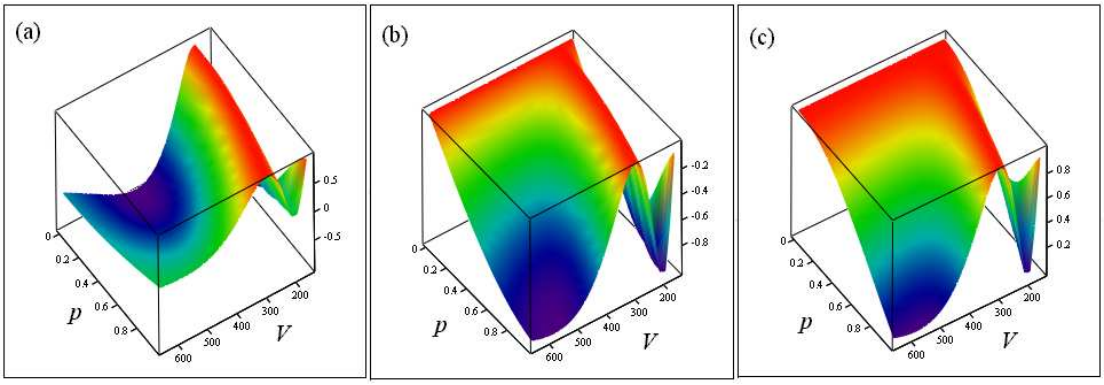

Fig. 1. Probability amplitudes as a function of the velocity and p. Surfaces (a) $a(V,p)$ and (b) $b(V,p)$ (or $a(V,p)$) if the initial state is $|100\rangle$ (or $|010\rangle$). (c) Surface $b(V,p)$, if the system is initially prepared in the $|010\rangle$ state. guneyF1.eps.

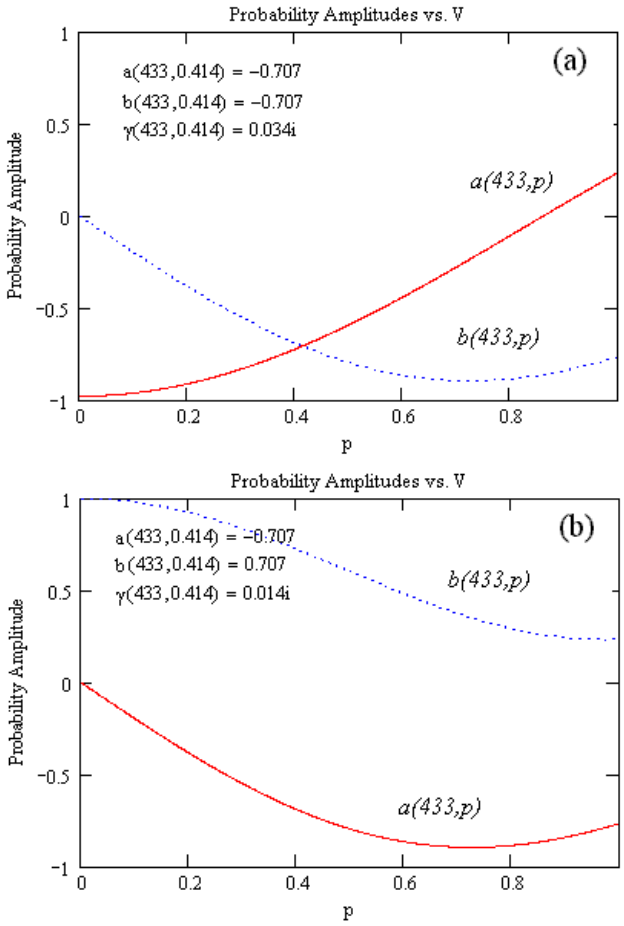

Fig. 2. Slices from each surface in Fig. 1. (a) Probability amplitudes $a(V,p)$—red—and $b(V,p)$—dashed blue—with $V = 433$m/s. The entangled state, Eq. (19), is obtained at $p = 0.414$. (b) Probability amplitudes $a(V,p)$—dashed blue—and $b(V,p)$—red—with the same velocity, $V = 433$m/s. The entangled state, Eq. (20), is observed at the same value, $p = 0.414$. guneyF2.eps.

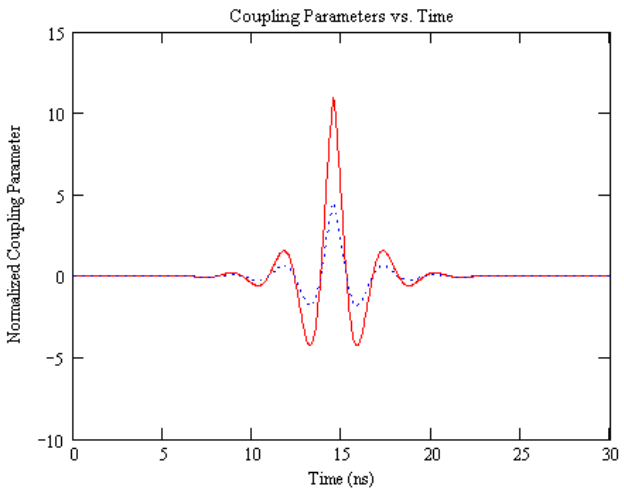

Fig. 3. Coupling parameters in the reference frame of moving atoms with velocities $V = 433\text{m/s}$ at $p = 0.414$. $\Omega_0 = 11 \times 10^9\text{Hz}$, $\omega = 2.4 \times 10^{15}\text{Hz}$, $l = 1.6\frac{\pi c}{\omega}$, $L = 10l$, $R_{\text{def}} = l.^6$ Atom A experiences the coupling parameter shown with the red solid curve and atom B the one shown with dashed blue. guneyF3.eps.

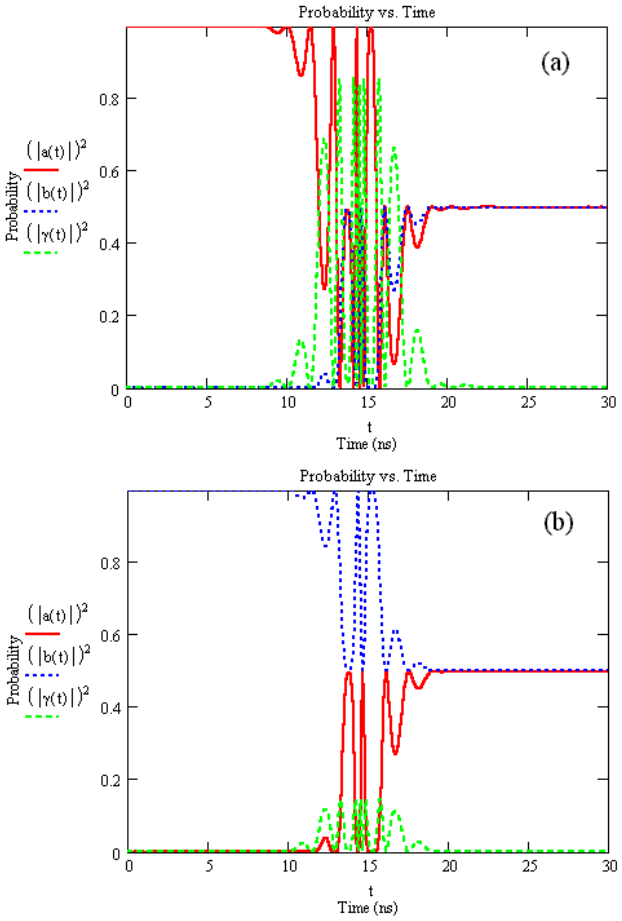

Fig. 4. Time evolution of the probabilities showing the final entanglement when (a) the initial state is $|100\rangle$ and (b) $|010\rangle$. guneyF4.eps.

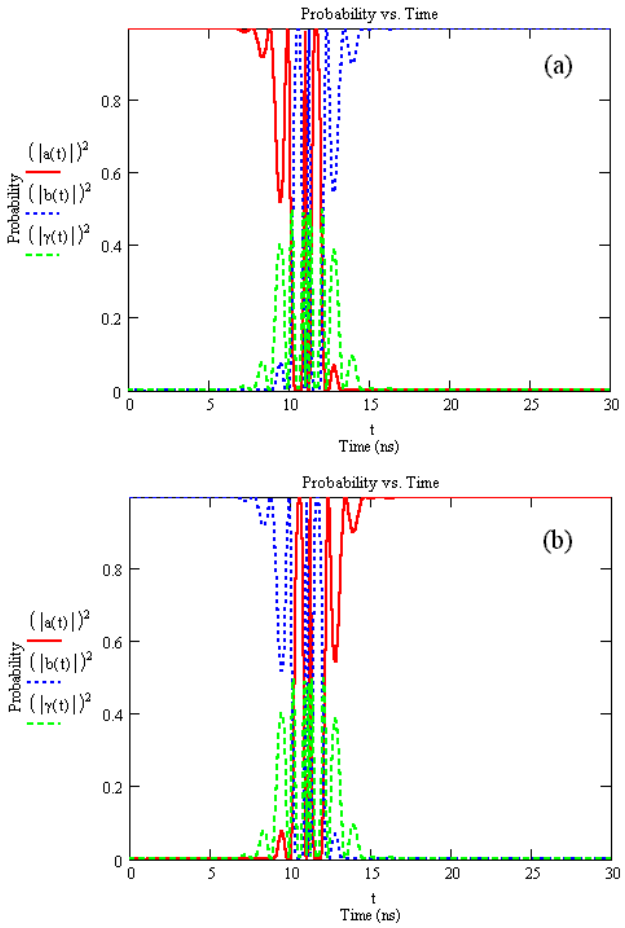

Fig. 5. Time evolution of the probabilities that leads to a dual-rail NOT (Pauli σ_x) logic operation when (a) the initial state is $|100\rangle$ and (b) $|010\rangle$. guneyF5.eps.

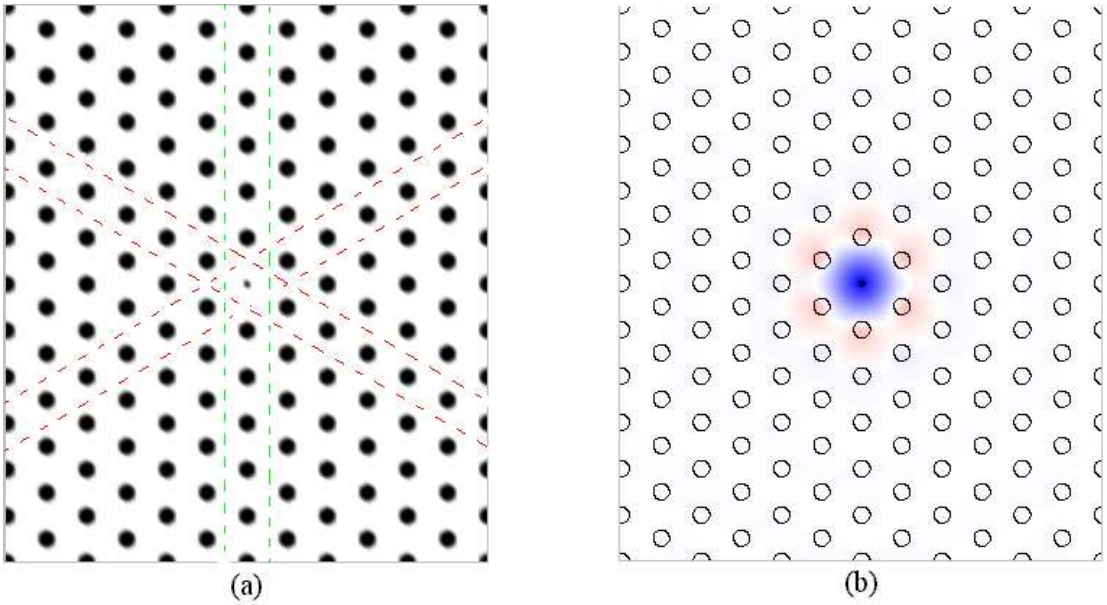

Fig. 6. (a) A single-mode microcavity in a 2D photonic crystal with a triangular lattice (see the text for details). (b) The corresponding electric field spatial profile for the transverse-magnetic (TM) mode allowed in the cavity. guneyF6.eps.

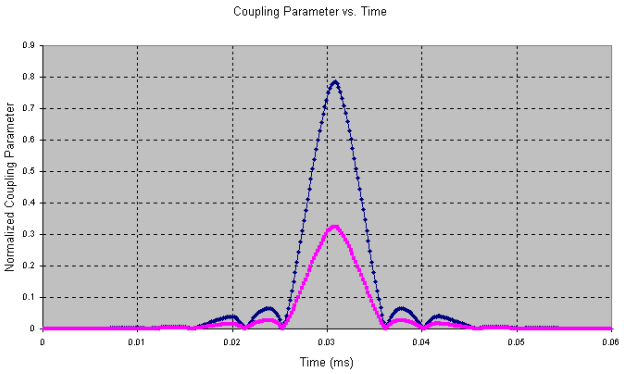

Fig. 7. Normalized coupling parameters (i.e., divided by g_0) in the reference frame of moving atoms with velocities $V = 374$m/s at $p = 0.414$, where g_0 is found to be 2.765MHz. Blue and red curves correspond to normalized coupling strengths for atoms A and B, respectively. guneyF7.eps.

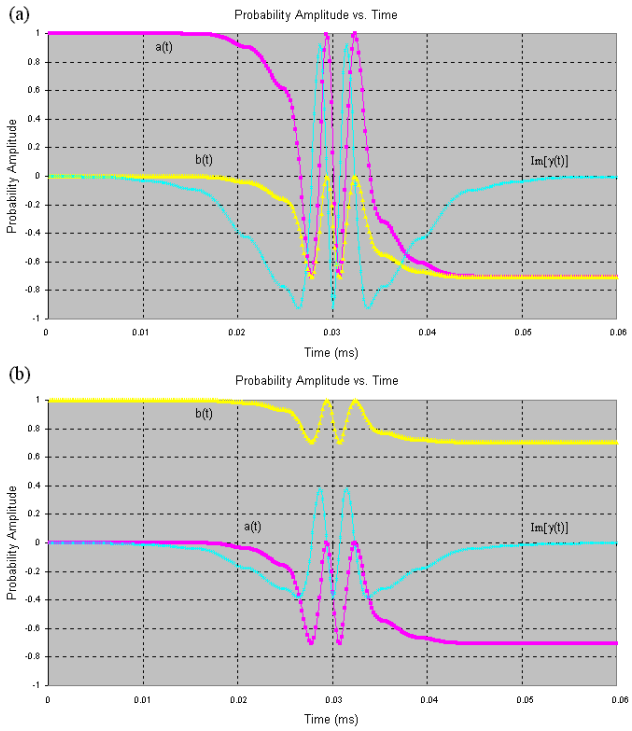

Fig. 8. Probability amplitudes for entangled atoms created by a dual-rail Hadamard operation in the 2D photonic crystal (see Fig. 6) (a) when atom A is initially in the excited state and (b) when atom B is initially in the excited state. $a(t)$, $b(t)$ and $\gamma(t)$ are probability amplitudes for the states $|100\rangle$, $|010\rangle$ and $|001\rangle$, respectively. guneyF8.eps.

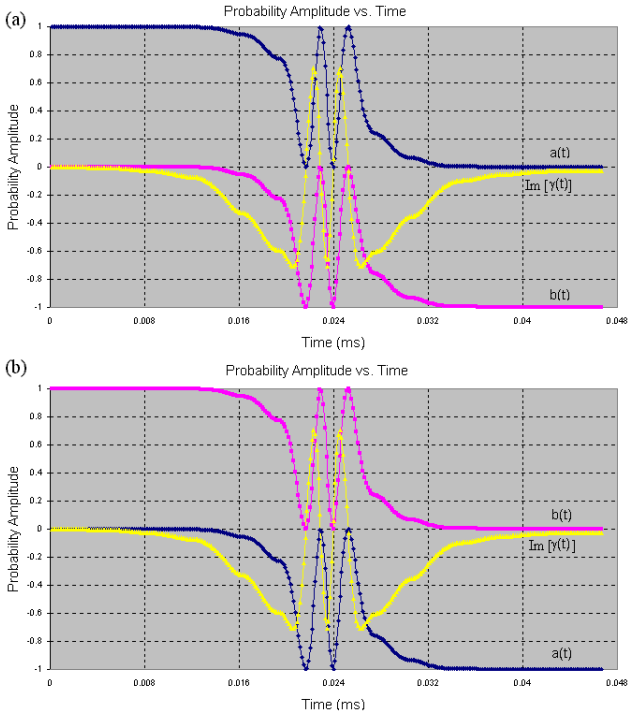

Fig. 9. Probability amplitudes for atom A and B under the dual-rail NOT operation in the 2D photonic crystal when initially (a) atom A is excited only and (b) atom B is excited only. guneyF9.eps.

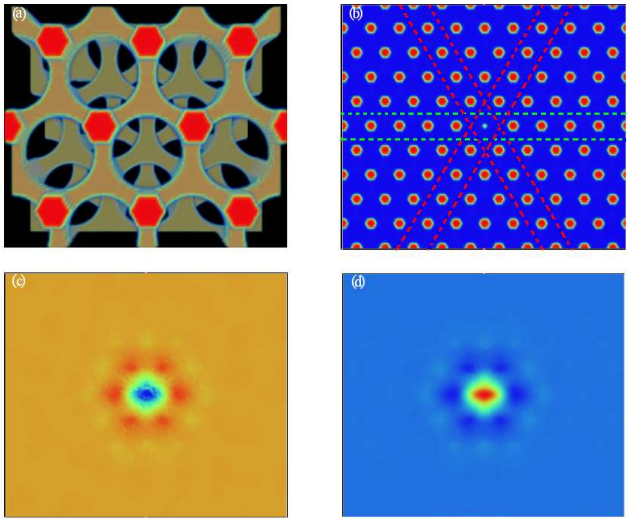

Fig. 10. (a) Top view of the 3D photonic crystal with fcc lattice. It consists of alternating layers of a triangular lattice of air holes and a triangular lattice of dielectric rods (for details of the structure, see Refs. [5, 22, 23]). The nearest-neighbor spacing within either a hole or rod layer is $\frac{1}{\sqrt{2}}l$, where l is the fcc lattice constant. The hole and rod radii are $0.293l$ and $0.124l$, respectively. The thicknesses of a hole layer and a rod layer are taken to be $0.225l$ and $0.354l$, respectively. Silicon is assumed as the high-index material of dielectric constant 12. (b) Horizontal cross-section of the crystal. Dashed lines show the obvious paths atoms can travel. In our simulations we assumed the path shown by the dashed yellow line. A defect is introduced by reducing the radius of the middle rod down to $0.050l$ to hold a single mode in the cavity. The (c) real part and (d) imaginary part of the electric-field of the TM mode allowed in the cavity at a particular instant in time with the frequency of $0.539c/l$. The imaginary part is half a period later. guneyF10.eps.

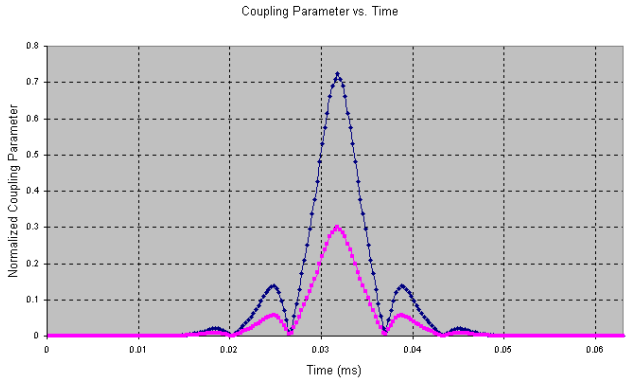

Fig. 11. Coupling parameters in the reference frame of the moving atoms with both velocities $V = 353\text{m/s}$, and $p = 0.414$, where g_0 is found to be 2.899MHz. Blue and red curves correspond to normalized coupling strengths for atoms A and B, respectively. guneyF11.eps.

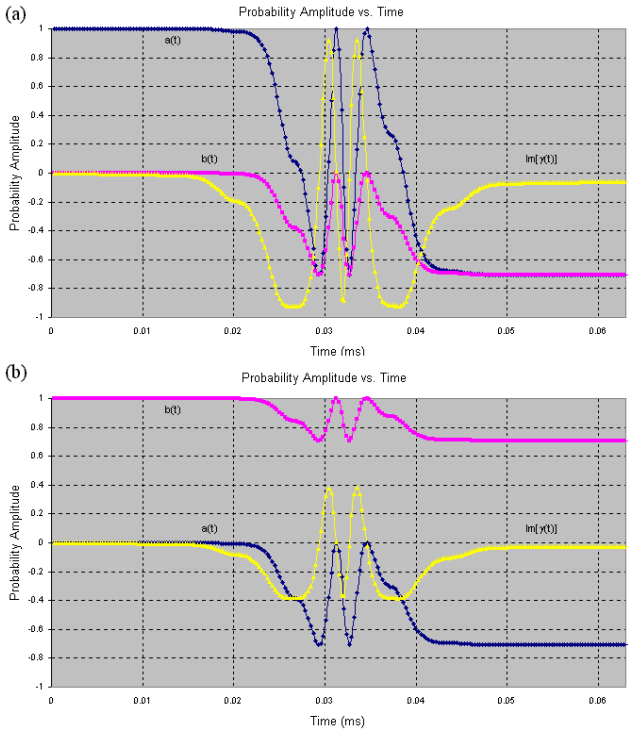

Fig. 12. Probability amplitudes for the entangled atoms under dual-rail Hadamard operation in the 3D photonic crystal (see Fig. 10) when (a) atom A is initially in the excited state and (b) atom B is initially in the excited state. $a(t)$, $b(t)$ and $\gamma(t)$ are probability amplitudes for the states $|100\rangle$, $|010\rangle$ and $|001\rangle$, respectively. guneyF12.eps.

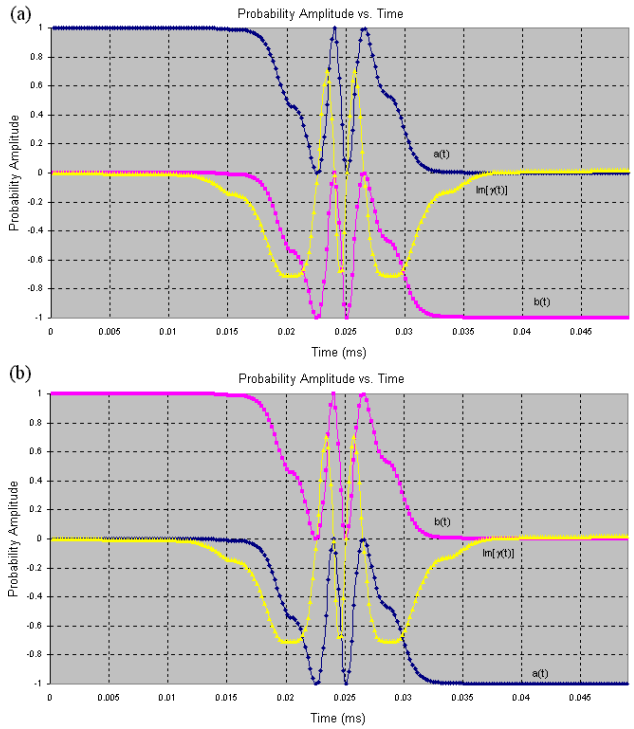

Fig. 13. Probability amplitudes for atoms A and B under the dual-rail NOT operation in the 3D photonic crystal when initially (a) only atom A is excited and (b) only atom B is excited. guneyF13.eps.